1776 *Biochemistry* **2010,** *49,* 1776–1786
DOI: 10.1021/bi901942m

BIOCHEMISTRY
including biophysical chemistry & molecular biology
Article

Investigation of the Binding Preference of Reovirus σ1 for Junctional Adhesion Molecule A by Classical and Steered Molecular Dynamics

B. Zhang,[‡,@] T. S. Lim,[⊥] S. R. K. Vedula,[§,@] A. Li,[§] C. T. Lim,[‡,§,∥,@] and V. B. C. Tan*[,‡]

[‡]*Department of Mechanical Engineering,* [§]*Division of Bioengineering, and* [∥]*Singapore-MIT Alliance, National University of Singapore, S117576 Singapore,* [⊥]*Singapore Immunology Network, S138648 Singapore, and* [@]*RCE in Mechanobiology, National University of Singapore, S117543 Singapore*

Received November 11, 2009; Revised Manuscript Received January 25, 2010

ABSTRACT: Biochemical studies have determined that reoviruses attach to cells by combining attachment protein σ1 to the binding interface of its receptor protein junctional adhesion molecule A (JAM-A), and the interface normally takes care of the homodimerization of JAM-A. Tighter binding and slower dissociation of for the σ1−JAM complex than for the JAM−JAM complex have been probed by both biological and atomic force microscopy experiments; however, the mechanism of the binding preference of the attachment protein for JAM-A still remains unclear. With the help of classical and steered molecular dynamics and energy calculations, the unbinding forces and kinetic properties of the complexes are investigated, together with detailed structural information analyses. A multireceptor mechanism is proposed for the binding preference, which can be helpful for future viral infection and vector targeting studies.

Viral infection is normally initiated by the attachment of a virus to specific host molecules on the cell surface. As attachment plays a crucial role in target cell selection in the infected host and is a critical determinant of viral disease outcome, it is a potential target for antiviral therapy (*1*). Although most infections are asymptomatic, reoviruses infect a broad range of mammalian hosts, including humans, and can cause mild gastrointestinal or respiratory illnesses, primarily in the very young (*2*). The mammalian reoviruses are deemed as highly useful experimental models for studying viral pathogenesis and show promise as vectors for oncolytics and vaccines (*3*). They usually attach to the host molecules by interactions between the reovirus attachment protein, σ1, and its receptor protein on the cell surface, junctional adhesion molecule A (JAM-A) (*4*−*6*).

Protein σ1 is a long molecule with an eight-stranded globular β-barrel head domain and a tail region with three β-spiral repeats (*7*−*9*). Recent crystal structures (*10*, *11*) indicate a trimer architecture of the protein and show that a prominent loop in the σ1 head contains a cluster of residues that are conserved among reovirus serotypes and form a binding site for JAM-A.

JAM-A is an integral membrane protein that belongs to the immunoglobulin (Ig) superfamily (*12*−*14*). The protein consists of two concatenated extracellular Ig-like domains (D1 and D2), a transmembrane region, and a short cytoplasmic tail (*15*, *16*). It predominately localizes at endothelial and epithelial cell tight junctions, on platelets, and, to a lesser degree, on the surface of leukocytes (*17*, *18*). It has been shown that homophilic JAM-A interactions play an important role in regulating both paracellular permeability and leukocyte transmigration (*12*, *19*−*21*). For instance, JAM-A influences the migration of leukocytes across endothelial and epithelial barriers in response to inflammatory cues (*22*). A very recent report indicates that JAM-A is a contributing factor in breast cancer cell invasion (*23*). The aggregation behavior experiments with the protein reveal that JAM-A assembles noncovalently to dimers (90%) in solution (*15*), and we suggest that the extracellular D1 domain is required for the homodimerization.

Recently, Guglielmi et al. (*11*, *24*) discovered that the σ1 protein of the reovirus attaches to the cell surface by disrupting the JAM-A homodimerization and the dissociation constant (K_D) of the interaction between σ1 and JAM-A is 1000-fold lower than that of the JAM-A−JAM-A (JAM−JAM hereafter) molecules, indicating that JAM-A strongly prefers σ1 as a ligand. These observations are further supported by our atomic force microscopy (AFM) unbinding force measurements of σ1−JAM-A (σ1−JAM hereafter) and JAM−JAM interactions (*25*). In the experiments, interactions were probed between trimer σ1 functionalized on an AFM tip and JAM-A protein transfected in L-fibroblast cells and expressed on the surface. The AFM results showed a much larger dissociation rate for the JAM−JAM complex ($0.688 \pm 0.349\ s^{-1}$) than for the σ1−JAM complex ($0.067 \pm 0.041\ s^{-1}$). A very recent crystal structure (*11*) displays an overall structure of a three-blade propeller topology for the σ1−JAM combination, with a σ1 trimer forming the hub and three D1 domains of JAM-A forming the blades. σ1−JAM and JAM−JAM interactions are analyzed and compared with each other. The authors explained why JAM-A has a higher affinity for σ1 than for another JAM-A by analyzing the protein−protein surface complementarities. The cavity in the JAM dimer interfaces usually contains water molecules that can significantly destabilize hydrogen bonds and salt bridges by lowering the dielectric constant of the medium, while the σ1−JAM complex possesses an almost perfect complementary interface. However, our energy decomposition calculations and kinetic investigations of the complexes appear to indicate a different mechanism for the protein binding preference.

Although the significant biophysical experiments demonstrate very important dynamic and kinetic evidence of the σ1−JAM

*To whom correspondence should be addressed. Telephone: 65-6516 8808. Fax: 65-6779 1459. E-mail: mpetanbc@nus.edu.sg.

 Published on Web 01/26/2010

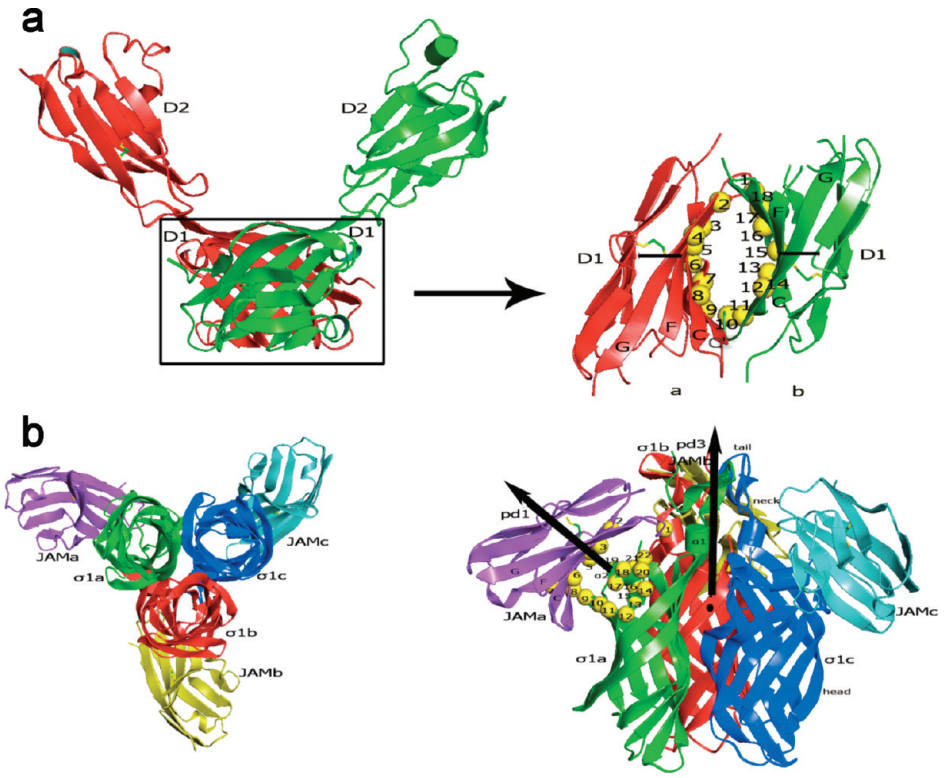

FIGURE 1: (a) D1D2−D1D2 JAM-A dimer (left) and truncated D1−D1 model (right). G, F, and C are β-sheets of JAM-A and named as described in ref *16*. (b) Structure of trimer σ1 and three pieces of JAM-As. The top view is on the left and the side view on the right. Pulling sites of both the complexes are depicted with numbered yellow balls, corresponding to those in Table 1. The pulling directions are shown with black arrows in both pictures. pd1 in panel b indicates the separation direction of the σ1−1JAM complex; the pulling direction of the σ1−2JAM complex, pd2, which points out of the paper, is drawn with the dark dot below the pd3 arrow, and pd3 describes the departure direction of the three pieces of the JAM-A proteins.

and JAM−JAM interactions, no atomic structural information of the interaction details is available. Unfortunately, the crystallography of the proteins offers only static snapshots of the protein−protein interactions; dynamic or kinetic details of the protein−protein adhesion process could not be probed. The mechanism behind the stronger binding affinity and the slower dissociation of the σ1−JAM complex than of the JAM−JAM complex, thus, still remain unclear. Normally, classical molecular dynamics (MD) is a powerful tool for understanding the properties of biosystems in which the internal motions and resulting conformational changes play an essential role in the interactions between ligands and receptors (*26*, *27*). However, with classical MDs, only systems in equilibrium can be explored (*28*−*30*). When molecules are not in equilibrium, such as when they are subjected to external loads, classical MDs will not be able or may need enormously long computational times to model the deforming molecule (*31*). In such situations, the classical method requires the implementation of new algorithms. Steered molecular dynamics (SMD) (*32*−*34*) applies time-dependent external force to manipulate biomolecules to facilitate, for instance, the unbinding of ligands from proteins, etc., while providing full atomistic details of the simulated process that are not usually available from experimental techniques, such as structure−function relationships of the ligand−receptor complex, conformational changes, and mechanisms of enzyme selectivity (*35*−*38*). We conducted classical and steered MDs, together with molecular mechanics-generalized Born/surface area (MM/GBSA) energy calculations, to investigate the mechanism of the protein binding preference of the JAM−JAM and σ1−JAM complexes on an atomic level and to explore the kinetic properties of the complexes under nonequilibrium conditions similar to those determined in AFM experiments (*25*−*30*). We performed energy decompositions to analyze the electrostatic and van der Waals (VDW) contributions from each amino acid in the complexes to examine the solvent effect on hydrogen bonding and salt bridges. Unbinding forces of the complexes from SMDs are then compared with the AFM experimental results to explain the binding affinity from the point of view of energy. Dissociation rates of the complexes are then calculated and presented to describe the binding preference from a kinetic perspective. The unbinding details are then examined to give atomic-level descriptions of the unbinding processes. Finally, on the basis of all the energetic, kinetic, and structural analyses, a multireceptor binding mechanism of the σ1 preference by JAM-A is proposed.

METHODS

Molecular Dynamics and Steered Molecular Dynamics Simulations. Both classical and steered molecular dynamics simulations were conducted using the AMBER9 program package (*40*) with the all-atom force field of Cornell et al. (*41*). The starting geometries for the simulations of the JAM−JAM and σ1−JAM complexes were initiated with the X-ray structure from the Protein Data Bank (PDB entries 1NBQ and 3EOY, respectively). The motifs in our model are named according to ref *16* and shown in Figure 1. The original structure of the JAM−JAM complex is also truncated to give a dimer consisting of only the D1 domains (Figure 1a), considering that all the crucial interactions reside between the D1 termini and the computational time of the smaller homodimer is less expensive than that of the D1−D2 dimer (the JAM−JAM dimer in the

Table 1: Pulling Sites of JAM−JAM and σ1−JAM Complexes

label of atom in Figure 1a	amino acid from domain a	label of atom in Figure 1a	atom from domain b	label of atom in Figure 1b	atom from JAMa	label of atom in Figure 1b	atom from σ1a
1	Gly115	10	Gly115	1	Gly115	9	Asp423
2	Tyr119	11	Tyr119	2	Arg59	10	Val371
3	Arg59	12	Glu121	3	Met110	11	Thr372
4	Glu121	13	Met110	4	Glu61	12	Gly373
5	Met110	14	Arg59	5	Tyr75	13	Leu374
6	Glu61	15	Glu61	6	Lys63	14	Leu375
7	Tyr75	16	Tyr75	7	Ala79	15	Pro376
8	Lys63	17	Lys63	8	Leu72	16	Pro377
9	Leu72	18	Leu72	−	−	17	Leu378
−	−	−	−	−	−	18	Leu379
−	−	−	−	−	−	19	Thr380
−	−	−	−	−	−	20	Gly381
−	−	−	−	−	−	21	Asp382
−	−	−	−	−	−	22	Thr383

following refers to the D1−D1 combination). A mutated JAM−JAM complex is also generated to compare the binding stability and kinetic properties with those of the original dimer. According to previous experiments (*24*), five key amino acids (Arg59, Glu61, Lys63, Tyr75, and Glu121) are individually required for stabilization of JAM−JAM dimers. Considering the sensitivity of the molecular dynamics methodology, all the amino acids in both monomers are mutated at the same time to give a mutated JAM−JAM (mJAM−JAM) complex.

All simulations are at neutral pH. Lys and Arg residues are positively charged, and Asp and Glu residues are negatively charged. The default His protonation state in Amber9 is adopted. Counterions are added to maintain the eletroneutrality of all the systems. The classical and steered MD systems are immersed in 10 and 40 Å layer truncated octahedron periodic boxes of TIP3P water molecules (*42*), respectively. The solvent box in the SMD simulations has to be sufficiently large to ensure the proteins remain enveloped by water molecules throughout the simulation while a reasonable computational time is maintained. A 2 fs time step is used in all the simulations, and long-range electrostatic interactions are treated with the particle mesh Ewald (PME) (*43*) procedure using a cubic B-spline interpolation and a 10^{-5} tolerance for the direct space and with a 12 Å nonbonded cutoff. Bond lengths involving hydrogen atoms are constrained using the SHAKE algorithm (*44*). All systems are minimized prior to the production run. The minimization, performed with the SANDER module under constant volume condition, consists of four steps. All heavy atoms in both proteins and ligands are restrained with degressive forces of 500, 100, and 5 kcal mol^{-1} Å^{-1}. In the first three steps, minimization of the solvent molecules and hydrogen atoms of the systems involves 250 cycles of steepest descent followed by 250 cycles of conjugate gradient minimization. All systems are then relaxed by 500 cycles of steepest descent and 1000 cycles of conjugate gradient minimization in the last step. The systems are then heated to 300 K in four steps. The systems are first heated to 100 K over 10 ps and then to 200 K over the next 10 ps, and then to 250 K over an additional 10 ps. Finally, they are heated to 300 K over the last 20 ps. The production parts of the classical MDs of the D1D2−D1D2 JAM dimer and the mJAM−JAM, JAM−JAM, and σ1−JAM complexes were carried out over 10, 10, 16, and 10 ns, respectively, in the NPT ensemble at 300 K with Berendsen temperature coupling and constant pressure (1 atm) with isotropic molecule-based scaling (*45*). A 150 ps equilibrium running is followed by the SMD simulations. In selecting the spring constant and rate of pulling, we gave due consideration to keeping the computational time practicable. If the spring constant is too small, the time needed to separate the complexes can be prohibitively long. A series of four different spring constants of 10, 20, 40, and 80 kcal mol^{-1} Å^{-2} are applied to separate the JAM−JAM, mJAM−JAM, trimer σ1 and one JAM (σ1−1JAM), trimer σ1 and two JAMs (σ1−2JAM), and σ1 and three JAMs (σ1−3JAM or σ1−JAM) complexes. The complexes are separated at a speed of 4 m s^{-1} until the distance between the proteins reaches 40 Å; i.e., the SMD simulation spans 1 ns. Although the pulling speed is much greater than those in our AFM experiments (*25*), it is within the range used in many reported SMD simulations (*46*−*49*). The mass centers of the major atoms forming intermolecular interactions between the proteins where the displacements are specified are shown in Figure 1 and listed in Table 1.

MM-GBSA Calculations. Energy decompositions of JAM−JAM and σ1−JAM complexes are analyzed using the MM-GBSA (*50*) approach to highlight the electrostatic and VDW contributions in the binding of the proteins.

The binding free energies (ΔG_{bind}) are computed as

$$\Delta G_{bind} = \Delta G(\text{complex}) - [\Delta G(\text{protein}) + \Delta G(\text{ligand})] \quad (1)$$

$$\Delta G_{bind} = \Delta E_{gas} + \Delta G_{solv} - T\Delta S \quad (2)$$

$$\Delta E_{gas} = \Delta E_{int} + \Delta E_{ele} + \Delta E_{vdw} \quad (3)$$

$$\Delta G_{solv} = \Delta G_{GB} + \Delta G_{nonpolar} \quad (4)$$

The sum of molecular mechanical energies, ΔE_{gas}, can be divided into contributions from internal energy (ΔE_{int}), electrostatic potential (ΔE_{ele}), and van der Waals potential (ΔE_{vdw}). The solvation free energy (ΔG_{solv}) is composed of two parts: polar solvation free energy (ΔG_{GB}) and nonpolar solvation free energy ($\Delta G_{nonpolar}$). All energies are averaged along the MD trajectories. The snapshots are sampled from the last 5 ns at intervals of 50 ps. The single-trajectory approach is applied to estimate the energies. Estimation of energies in this manner has proven to be successful in our previous work and many other studies (*31*−*35*). Part of the reason for the success of this approach is the cancellation of errors that hides the effect of incomplete sampling. A better approach is the use of separate trajectories for the protein−ligand complex, free protein, and free ligand. Unfortunately,

because of sampling limitations, the separate trajectory approach appeared to be significantly less stable. E_{gas} is obtained using SANDER, and estimation of ΔG_{GB} was conducted with a built-in module, PBSA in AMBER. $G_{nonpolar}$ was determined with eq 5

$$\Delta G_{nonpolar} = \gamma A + b \quad (5)$$

where A is the solvent-accessible surface area estimated using Sanner's algorithm (*51*) with a solvent probe radius of 1.4 Å and the PARSE atomic radius parameters (*52*). γ and b are empirical constants and are set to 0.00542 kcal mol^{-1} Å^{-1} and 0.92 kcal/mol, respectively.

Bell's Model. Bell's model linearly correlates the rupture force and logarithm of the applied loading rate (eq 6) (*53*, *54*). It has been widely used to characterize the dynamics of the dissociation process between biomolecules (*55*, *56*)

$$F_R = \frac{k_B T}{x_b} \ln \frac{F' x_b}{k_B T k_{off}} \quad (6)$$

where k_B is Boltzmann's constant, T is the absolute temperature, x_b is the distance between the bound state and the energetic maximum, $F' = kv$ is the loading rate (k is the spring constant and v the velocity), and k_{off} is the kinetic rate of binding dissociation at equilibrium.

The rupture force (F_R) and the logarithm of the loading rate [ln(kv)] correlation is determined via least-squares linear regression. Since the original instantaneous force has too much fluctuation, the unbinding forces are examined at 10 ps intervals. This interval is selected because it allows examinations of the trajectory without the maximum unbinding force significantly deviating from the value by visual inspection of force versus reaction coordinate.

RESULTS

Validation of the Truncated JAM−JAM Model from both Structural and Energetic Perspectives. According to the experiments of Kostrewa and Prota et al. (*15*, *16*), the JAM homodimer interface includes four buried salt bridges, as well as several hydrophobic contacts that are responsible for the combination of the dimer. The root-mean-square deviation (rmsd) values of the D1D2−D1D2 dimer and the distances of crucial interactions between monomers (Arg59−Glu61, Glu61−Arg59, Lys63−Glu121, Glu121−Lys63, Leu72−Tyr119, Tyr119−Leu72, and Met110−Met110) are shown in Figure 2. Comparing the smooth D1 domain rmsd values with that of the oscillatory curves of the monomers (D1D2) and dimer (D1D2−D1D2), we find that the fluctuation of the dimer in the 10 ns MDs seems to be mainly introduced by the swinging of the D2 domains. Considering the computational cost and the unit responsible for the interactions is mainly D1, the stability and symmetry of D1−D1 binding are then explored by long time MDs with both the D2 domains excluded. The rmsd of the D1−D1 dimer and the distances of the important interactions (Arg59−Glu61, Glu61−Arg59, Lys63−Glu121, Glu121−Lys63, Leu72−Tyr119, Tyr119−Leu72, and Met110−Met110) are depicted in Figure 3. It turns out the dimer remains stable throughout the dynamic process. The crucial interactions are as stable as those in the D1D2−D1D2 complex. In addition, the computation is much faster than the calculations in which the D2 domain dimer is involved. The "dimer" refers to the D1−D1 complex in the following context.

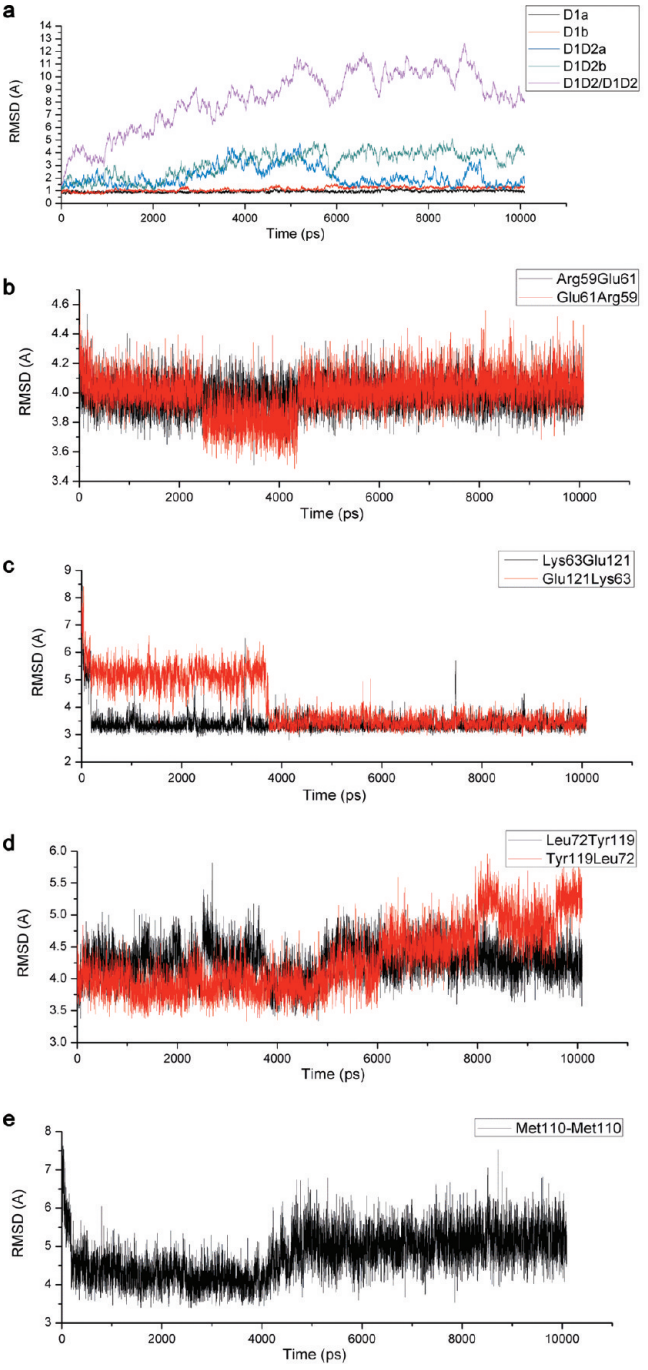

FIGURE 2: (a) rmsd of the D1D2−D1D2 JAM-A dimer and of the D1 and D1D2 domains. (b−e) Plots of distance vs time during the 10 ns classical MDs for (b) Arg59−Glu61 and Glu61−Arg59, (c) Lys63−Glu121 and Glu121−Lys63, (d) Leu72−Tyr119 and Tyr119−Leu72, and (e) Met110.

On the basis of Guglielmi's selected point mutation experiments (*24*), the five amino acids (Arg59, Glu61, Lys63, Tyr75, and Glu121) important for the homodimerization of the JAM dimer on the protein interface are mutated to alanine to validate the accuracy and applicability of the energy calculations in this work. Our MM/GBSA calculations show that the binding is greatly impaired by the mutations, as reflected by the binding energies of −46.28 and −75.73 kcal/mol for the mutated and original dimers, respectively. Although the mutated monomers adhere to each other without any obvious dissociation during the dynamic process, the mutations in the dimer model seem to be consistent with the experimental results, which indicated that

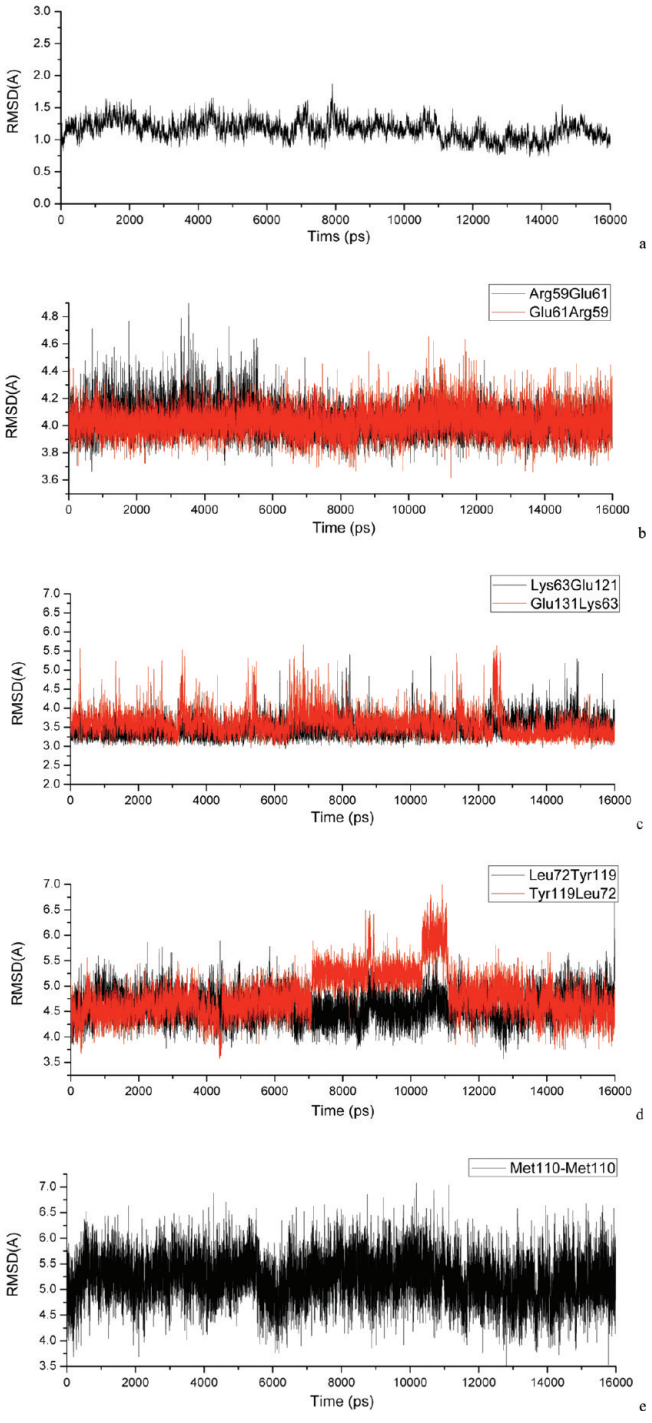

FIGURE 3: (a) rmsd of the D1−D1 JAM-A dimer. (b−e) Distance vs time plots from classical MD.

mutation of the five residues alters the capacity of JAM to form dimers. The calculations, thus, verify the correctness of the model in terms of binding energy.

A Comparison between JAM−JAM and σ1−JAM Binding. The hydrogen bonding (HB) and van der Waals (VDW) contributions from amino acids on the JAM−JAM and σ1−JAM interfaces are identified and listed in Table 2. From the table, it is evident that both the complexes are combined via extensive HB and VDW interactions. Considering HB drives strong noncovalent interactions and that there are more HB contributions in the JAM−JAM complex (12) than in the σ1−JAM complex (9), it seems, from a purely chemical point of view, that the homodimer possesses stronger interactions. Nevertheless, it has been previously proposed that the σ1−JAM complex binds much more strongly than the JAM−JAM complex, and the water molecules in the cavity between the homodimer are the main reason for the impaired binding affinity (*11*). Nevertheless, the energy decomposition results in Table 3 show that contributions from the amino acids of JAM in both the complexes appear very close when the solvent influences are taken into account. This suggests that the water environment does not strongly affect the electrostatic interactions. Moreover, considering the crystal structure of the trimer σ1 unit complex with three JAM molecules, the interactions within the σ1−JAM complex could be greatly enhanced when the attachment protein approaches the cell surface and is captured by three receptor proteins rather than by one or two JAM molecules. To elucidate and compare the bindings of different combinations of σ1−JAM complexes, the unbinding force profiles of σ1−1JAM, σ1−2JAM, and σ1−3JAM complexes by SMD simulations with a spring constant of 10 kcal mol^{-1} $Å^{-2}$ and a pulling velocity of 4 ms^{-1} were conducted. For comparison, the rupture forces of JAM−JAM and mJAM−JAM complexes are plotted in Figure 4 and listed in Table 4.

As seen for the force profiles and the tabulated values, the maximum force is ~1400 pN when only one JAM is pulled away from the trimer unit. This is obviously smaller than that of the JAM−JAM separation force (~1700 pN). Hence, the binding between the trimer and a single JAM seems weaker than JAM−JAM binding. When two JAMs are dragged away, the maximum rupture force is approximately on the same order of magnitude as that of the JAM−JAM complex (~1750 pN). At the instance when all the three pieces of JAM leave the trimer, the rupture force appears to be much greater than that of the former two and the JAM−JAM complex (~3400 pN), and the force profile with three peaks distinctly differs from that of the homodimer, which will be discussed later. Among the three types of σ1−JAM combinations, it seems only the results of the last complex agree with our AFM experiments (*25*), in which the measured unbinding forces of the σ1−JAM complex are greater than those of the JAM−JAM complex until the loading rate reaches a certain degree, as shown in Figure 5. Also, it quantitatively confirms the hypothesis of Kirchner et al. (*11*) that the σ1 trimer could simultaneously engage more than one JAM-A monomer. A similar trend in the force versus loading rate relationship is also produced by our simulations. Therefore, the SMD unbinding force results seem to imply the stronger binding of the σ1−JAM complex compared to that of the JAM−JAM complex is due to the attachment of σ1 to multiple receptor proteins.

In the case of JAM−JAM and mJAM−JAM complexes, the maximum unbinding force of the mutated dimer (~700 pN) is smaller than the original (~1700 pN), as expected (Figure 4), which again verifies the importance of the five amino acids in the binding and validates the JAM−JAM model.

According to Bell's model (*53*) and the extended discussions about the dissociation rate (*37*, *54*, *57*) ,the off rate increases exponentially with force when forces are applied at high rates. Normally, the rupture forces from SMD simulations (*37*, *39*, *54*, *57*, *58*) are larger than those from AFM measurements (*25*, *39*, *54*, *57*), mainly due to the much higher loading rates applied in the calculations (usually in newtons per second to make the computation practicable) than in the experiments (in piconewtoms per second). As a consequence, the experimentally applied and calculated forces and dissociation rates are in different

Table 2: Hydrogen Bonding (HB) and van der Waals (VDW) Interactions at the Interfaces of JAM−JAM and σ1−JAM Complexes

atom of JAMa	atom of JAMb	type of interaction	atom of JAM	atom of σ1	type of interaction
Gly27 O	Thr69 OG1	HB	Gly115 O	Arg316 NH1 (NH2)	HB
Thr69 OG1	Gly27 O	HB	Arg59 NH1 (NH2)	Asp382 OD1 (OD2)	HB
Thr70 O	Tyr119 OG1	HB	Arg59 NH1 (NH2)	Gly381 O	HB
Tyr119 OG1	Thr70 O	HB	Glu61 OE1 (OE2)	Thr380 N	HB
Ser82 OG	Asn117 OD1	HB	Glu61 OE1 (OE2)	Thr380 OG1	HB
Asn117 OD1	Ser82 OG	HB	Lys63 NZ	Thr380 OG1	HB
Arg59 NH1 (NH2)	Glu61 OE1 (OE2)	2HB	Asn76 ND2	Gly381 O	HB
Glu61 OE1 (OE2)	Arg59 NH1 (NH2)	2HB	Asn76 ND2	Glu384 OE1 (OE2)	HB
Lys63 NZ	Glu121 OE1 (OE2)	HB	Ala81 N	Asp423 OD1 (OD2)	HB
Glu121 OE1 (OE2)	Lys63 NZ	HB	Glu114	Tyr298	VDW
Leu46	Try119	VDW	Tyr119	Pro376	VDW
Try119	Leu46	VDW	Tyr119	Pro377	VDW
Tyr75	Gly115	VDW	Ser112	Leu379	VDW
Gly115	Tyr75	VDW	Met110	Leu379	VDW
Met110	Met110	VDW	Leu72	Gly424	VDW
–	–	–	Leu72	Val425	VDW

Table 3: Energy Decomposition Results for Amino Acids at the Interfaces of JAM−JAM and σ1−JAM Complexes

amino acid from Jam in the JAM−JAM complex	E_{GB} (kcal/mol)	amino acid from JAMa in the σ1−JAM complex	E_{GB} (kcal/mol)
Arg59	−122.86	Arg59	−121.34
Glu61	−78.62	Glu61	−78.15
Lys63	−1.71	Lys63	0.18
Tyr75	1.06	Tyr75	1.81
Met110	−8.38	Met110	−8.09
Gly115	5.00	Gly115	5.13
Tyr119	11.89	Tyr119	12.15

regimes (*37*, *54*, *57*). Although MD simulations of rupture processes cannot attain experimental force and time scales currently, it has been shown in many cases (*37*, *39*, *56*−*58*) that SMD simulations match qualitatively the results of AFM experimental characterization. Rather than a comparison of actual numbers of the calculated dissociation rate with the AFM measurements, the relative magnitude of the calculated k_{off} of all the systems in this work is used for comparisons of the dissociation of the complexes. To evaluate the dissociation rates of the complexes with Bell's model, three more spring constants of 20, 40, and 80 kcal mol^{-1} Å^{-2} are applied to separate JAM−JAM, mJAM−JAM, σ1−1JAM, σ1−2JAM, and σ1−JAM complexes. The relationships of unbinding force F_R and logarithm of loading rate (kv) are shown together with the dissociation rates (k_{off}) in Table 4 and Figure 6.

The ∼55-fold higher dissociation rate of the mJAM−JAM complex compared to that of the original homodimer describes a much faster dissociation of the complex in solution. This is in agreement with reported experimental results (*24*) that the protein does not show the presence of aggregates when the crucial amino acids are mutated. The dissociation rate of the σ1−JAM complex is ∼1300 times lower than that of the JAM−JAM complex, indicating a much slower release of σ1 from the receptors. This agrees well with the AFM results, which gave dissociation rates of 0.067 and 0.688 s^{-1} for the σ1−JAM and JAM−JAM complexes, respectively. However, comparison of the dissociation rates of the σ1−1JAM, σ1−2JAM, and σ1−JAM complexes yields several interesting observations. The dissociation rate of the σ1−1JAM complex (9.91 × 10^8 s^{-1}) indicates a faster release of the attachment protein compared to that for release of JAM from a single JAM receptor (2.19 × 10^8 s^{-1}). When two receptor proteins are involved in binding, the dissociation rate of the σ1−2JAM complex (4.11 × 10^8 s^{-1}) is obviously lowered and closer to the JAM−JAM dissociation level. The system that includes all the three JAMs and σ1 exhibits the slowest dissociation (2.87 × 10^5 s^{-1}). Together with the unbinding force discussions of the complexes, it seems the multireceptor binding of the attachment protein not only introduces stronger interactions but also results in slower dissociation. To understand why this is so requires an analysis of the structural details and unbinding force profiles.

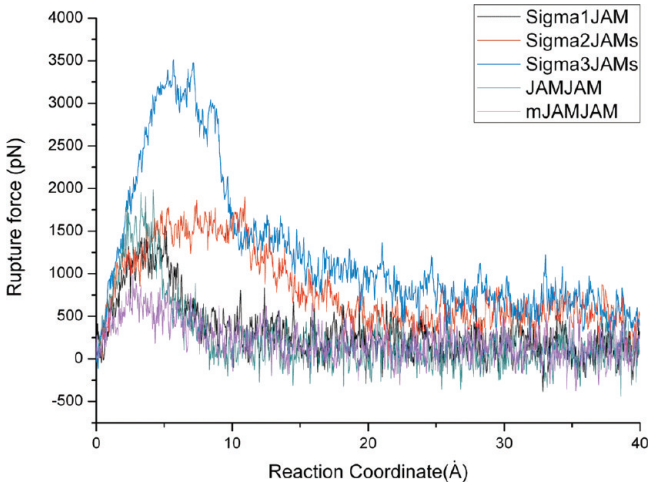

FIGURE 4: SMD results of rupture force vs reaction coordinate for σ1−1JAM (Sigma1JAM), σ1−2JAM (Sigma2JAMs), σ1−3JAM (Sigma3JAMs), JAM−JAM, and mJAM−JAM complexes, where the spring constant and velocity are 10 kcal mol^{-1} Å^{-2} and 4 ms^{-1}, respectively. The reaction coordinate here represents the goal distance assigned to the systems.

Finally, the slope of the σ1−JAM force versus loading rate regression (262.5) is slightly smaller than that of the JAM−JAM regression (272.7). This implies that along with the increase in the loading rate, the two lines in Figure 6 will intersect with each other in the same manner as shown by AFM data (Figure 5).

Structural Details and Energy Profiles upon Separation of the JAM−JAM and σ1−JAM Complexes. The structural details of the unbinding processes, normally impossible to detect

Table 4: Dissociation Rates (k_{off}) of Complexes from Bell's Model

complex	maximum rupture force[a] (pN)				f_b[b] (pN)	R[b]	k_{off}[b] (s^{-1})
	3.3322 N/s	4.0254 N/s	4.7185 N/s	5.4117 N/s			
mJAM−JAM	735	910	1225	1540	393.9	0.992	1.21×10
JAM−JAM	1715	1820	2030	2275	272.7	0.986	2.19×10^8
σ1−1JAM	1400	1750	1610	2100	324.6	0.982	9.91×10^8
σ1−2JAM	1750	1925	2030	2450	318.1	0.957	4.11×10^8
σ1−3JAM	3430	3500	3640	3990	262.5	0.943	2.87×10^5

[a]Loading rate in logarithm, where spring constants are 10, 20, 40, and 80 kcal mol^{-1} $Å^{-2}$ and the pulling velocity is 4 ms^{-1} (1 kcal mol^{-1} $Å^{-2}$ = 7×10^{13} pN/m). [b]The relationship between the rupture force (piconewtons) and loading rate (piconewtons per second) is deduced according to Bell's model (eq 6), where $f_b = (k_B T)/x_b$ is the slope (thermal force), R the correlation coefficient, and k_{off} the dissociation rate.

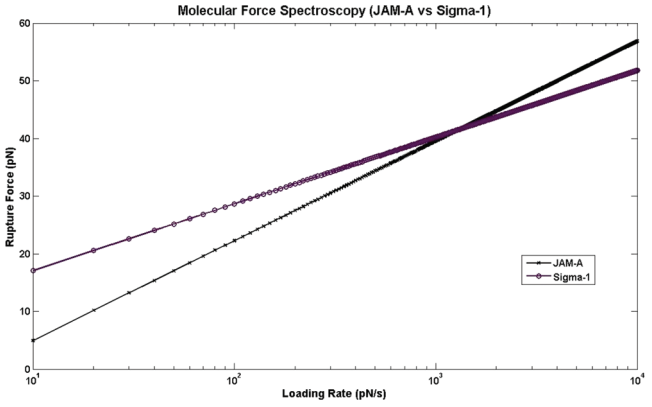

FIGURE 5: AFM experimental results of rupture force vs loading rate.

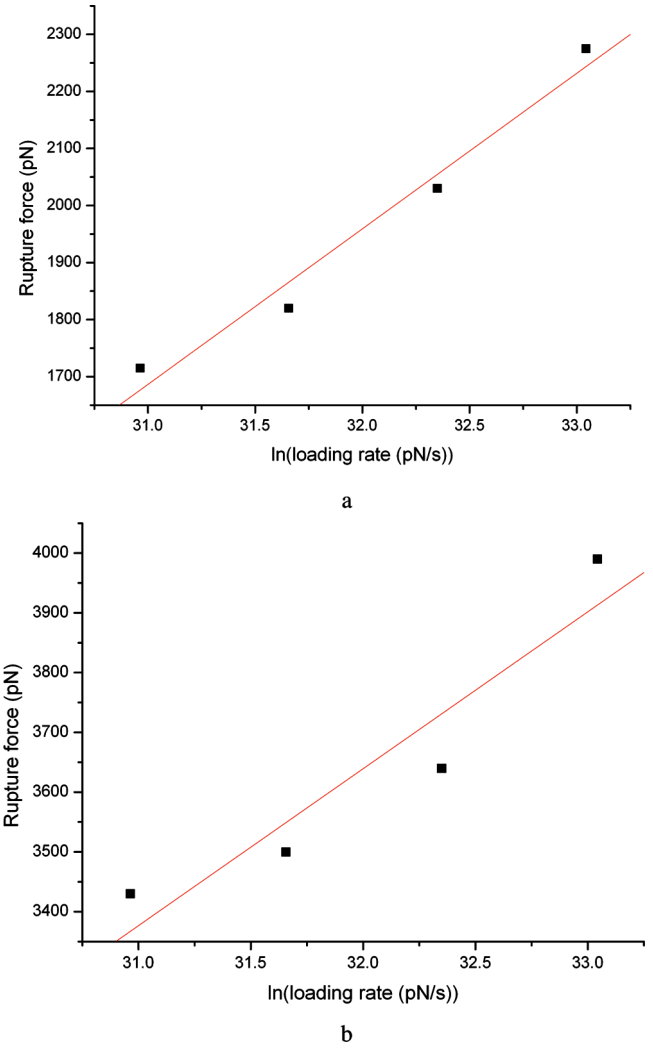

FIGURE 6: SMD results of rupture force vs loading rate: (a) JAM−JAM and (b) σ1−JAM.

by AFM experiments, are provided by the simulations, which are critical for understanding the mechanism of the stronger binding and slower dissociation of the σ1−JAM complex. HBs are first analyzed for the separation of JAM−JAM and σ1−JAM complexes. The separation distance versus reaction coordinate and unbinding force of several selected HBs are shown in Figure 7. From the figure, it is evident that the HBs appear to be very stable at the beginning of the pulling, increasing in length abruptly and almost linearly after some time. The sudden increase in the distances implies the breaking of the HBs between the amino acids. Also, it is clear from the figure that the increase and subsequent decrease in force are consistent with bond stretching and breaking. By comparing the bond breaking along the reaction coordinate, we found that the breaking of the bonds of the JAM−JAM complex occurs when the monomers are separated by a distance of 3−5 Å; however, the ruptures in the σ1−JAM complex happen when the proteins are ~7−10 Å apart. This raises the question of whether and why bond rupture in the JAM−JAM complex is earlier (or faster) than that of the σ1−JAM complex. This is answered by studying the structural properties of the two complexes. The interface of the JAM−JAM complex consists mainly of rigid β-sheets, and most of the amino acids responsible for the binding are located on these sheets, except for Try49 and Ala89, which reside on the loop between β-sheets F and G and the loop preceding β-sheet C′, respectively (Figure 1a). While the σ1−JAM interface involves rigid β-sheets C, F, and G of JAM, the tail, neck, and loop motifs of σ1 are highly flexible. Two α-helices (α1 and α2 in Figure 1b), one on the loop and the other on the neck, are also included in the interactions and found to be preceded and followed by flexible loops, indicating the helices can be easily displaced from their original positions. When the properties of the different interaction interfaces are compared, it is easy to understand the different bond breaking behaviors: the rigid β-sheets do not seem to undergo any large distortion when the JAM monomers are being pulled apart, so the bonds between them break quickly and the adhesion is weakened accordingly. On the other hand, the flexible interface of the σ1−JAM complex is deformed significantly. When the complex is being pulled apart, the flexible loops afford relatively larger conformational changes to keep the formation by the elongation of the bonds. As a result, the adhesion between the ligand and receptor proteins is more ductile. The obvious

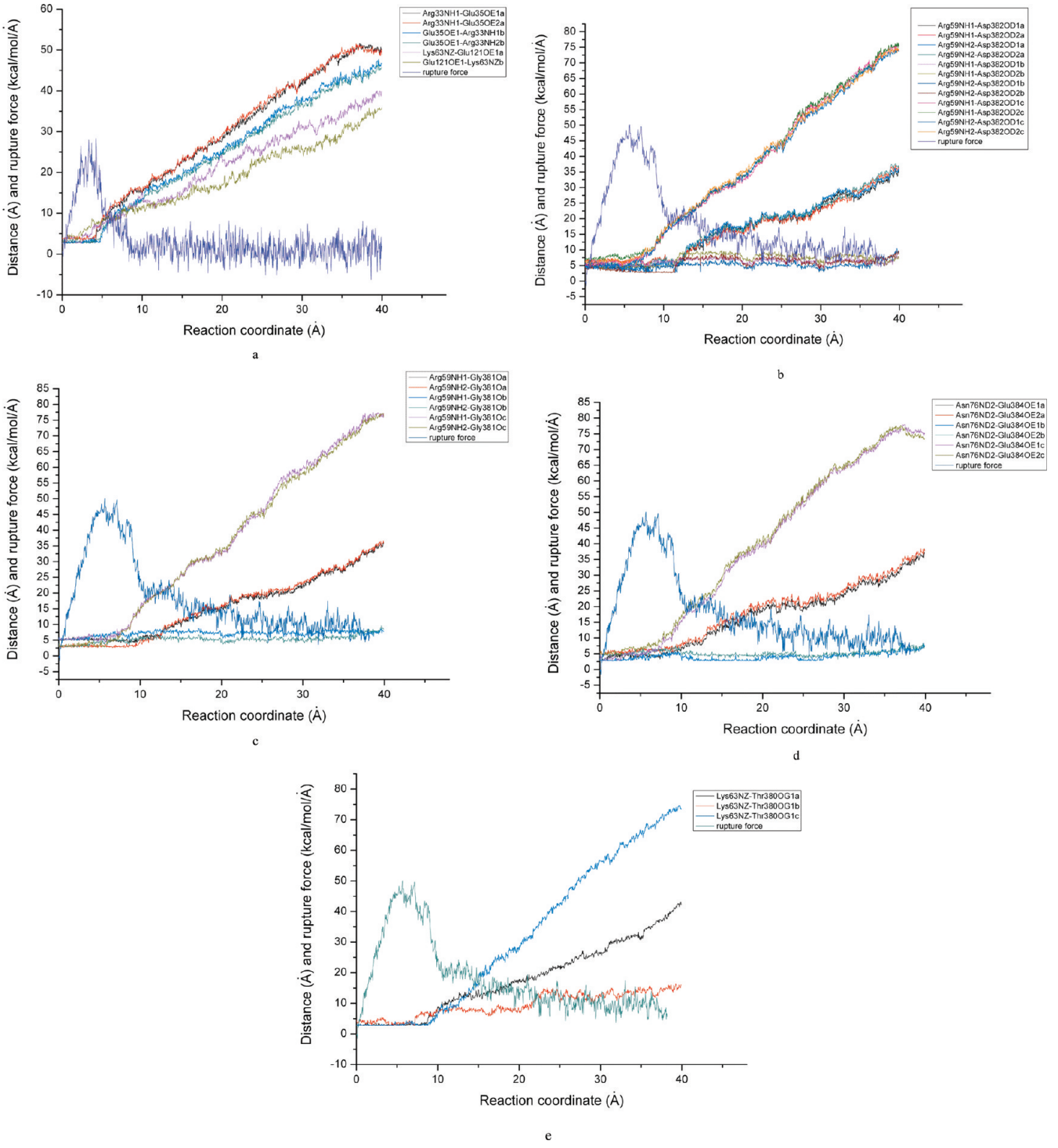

FIGURE 7: Separation distance and force profiles of selected HBs in both JAM−JAM (a) and σ1−JAM (b) complexes. Rupture force profiles are given for comparison of the force increase and decrease processes with bond stretching and breaking. The unit of kilocalorie per mole per angstrom is used for rupture force instead of the unit of piconewtons as in Figure 4 to give similar magnitudes for the forces and distances (1 kcal mol^{-1} $Å^{-1}$ ≈ 70 pN) because the vertical axis is for both force and distance.

fluctuations of the rmsd curves of the loop area in the three σ1 monomers can help to elucidate the large distortions in the motifs during the unbinding (Figure 8).

One more interesting observation about the bond splitting is that the HBs between the counterpart amino acid pairs in the different σ1−JAM interaction sets (the different molecules of σ1 and combined JAM are termed σ1a−JAMa, σ1b−JAMb, and σ1c−JAMc for the sake of clarity) are broken at different times and show distinct extension characteristics (Figures 7 and 9). In addition, three peaks are detected in the force curve of the σ1−JAM complex, unlike the unbinding force profile of the JAM−JAM complex (Figure 4). The snapshot of our SMD in Figure 9 describes a moment of the separation. Obviously, from the figure, the departures of the JAM proteins do not seem to happen simultaneously. This explains why the corresponding HB in the σ1a−JAMa, σ1b−JAMb, and σ1c−JAMc complexes break at different times and extend differently. From a modeling point of view, the trimer σ1 and three-JAM molecular crystal

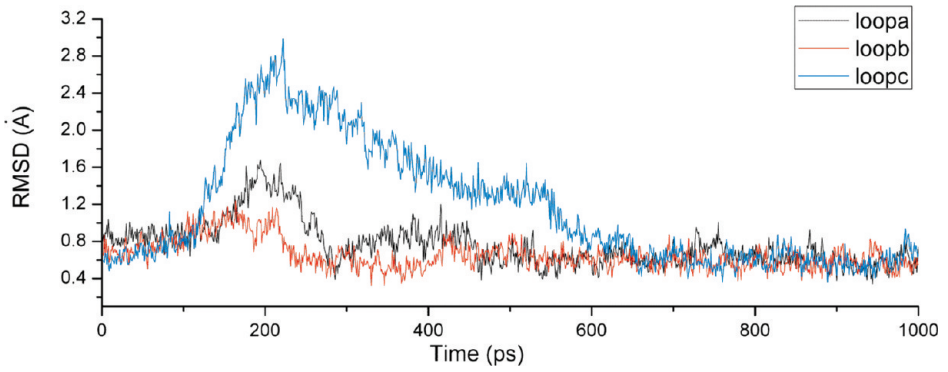

FIGURE 8: rmsd of the loop in σ1 interacting with JAMs. Loop a, loop b, and loop c are in σ1a−JAMa, σ1b−JAMb, and σ1c−JAMc complexes, respectively.

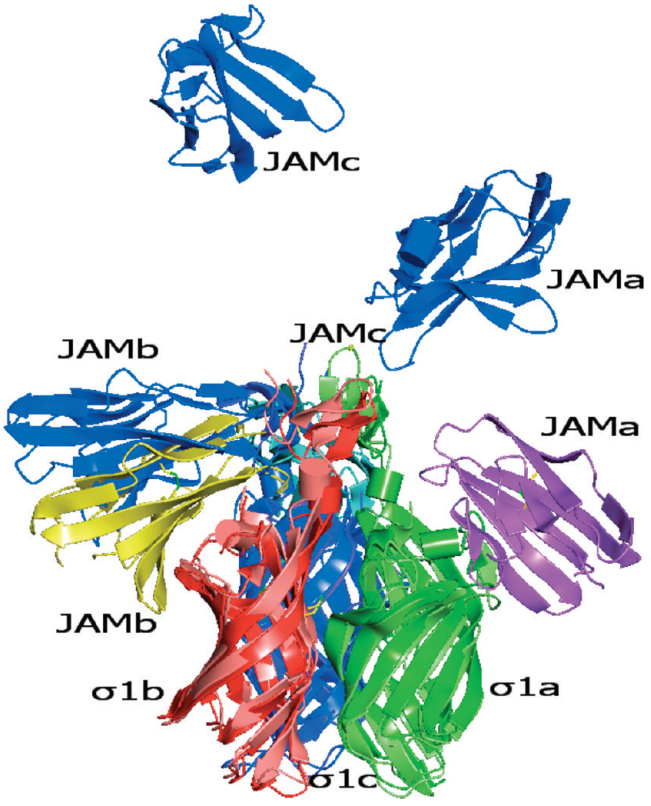

FIGURE 9: Superimposition of a snapshot of the σ1−JAM complex during the pulling and the original structure. The three JAM proteins, which are being pulled away from σ1 (JAMa, JAMb, and JAMc), are colored blue; the initial structures of JAMa, JAMb, and JAMc are colored purple, yellow, and green, respectively.

configuration is approximately, but not strictly, geometrically symmetric. The mass center of such a quasi-symmetrical system does not seem to superpose exactly with that of a perfectly symmetric σ1−JAM complex. Thus, when the pulling direction in the SMDs is set along the *Z*-axis as depicted in Figure 1b, it is not possible to be along the symmetric σ1−JAM *Z*-axis. Any slight deviation in the pulling direction leads to asymmetrical applications of the pulling forces on the bonds in σ1a−JAMa, σ1b−JAMb, and σ1c−JAMc complexes. The asymmetrical forces consequently break the bonds in different σ1−JAM sets asynchronously. On the other hand, the irregular breaking of the bonds might reflect the actual experimental details (*25*) or even the actual biological nature of separating the ligands from the receptors. In the AFM experiments (*25*), σ1 is attached on the cantilever tip by linking it to exposed COOH groups on the protein surface; i.e., the pulling points are not on the protein mass center. Thus, the pulling forces on the bonds in σ1a−JAMa, σ1b−JAMb, and σ1c−JAMc complexes do not appear to be symmetrical or uniform. As a result, the three JAM proteins leave σ1 in sequence. Additionally, it also seems difficult for a protein like σ1 in a dynamic biological environment to shift away from its receptors by breaking all bonds exactly at the same time. Except for the HB breaking evidence in Figure 7, the three continuous departures are also reflected by the three peaks along the force curves of the σ1−JAM separation.

DISCUSSION

The SMDs show the unbinding force of the σ1−JAM complex is stronger than that of the JAM−JAM complex only when two or three JAM molecules are involved in the binding with σ1. The calculated dissociation rates of the σ1−1JAM and σ1−2JAM complexes are around the same order of magnitude as that of the homodimer, but the σ1−3JAM complex dissociates much more slowly than the JAM−JAM complex. The simulations, therefore, not only agree with existing experimental findings of tighter binding and a slower dissociation rate for the σ1−JAM complex than for the JAM−JAM complex but also indicate a multireceptor binding mechanism of the binding preference of the homodimerization interface of JAM for σ1 than for JAM. The structural details evidently show that the HBs in the σ1−JAM complex are more ductile than those in the JAM−JAM complex when the complexes are pulled apart due to the flexible interaction interfaces between σ1 and JAMs. Furthermore, the observations that the HBs between the counterpart amino acid pairs break at different times and extend distinctly and the three peaks along the unbinding force profile of the σ1−JAM complex suggest that the three JAMs leave σ1 at different times. Together with the report that the JAM dimer interface is dynamic, which is thought to facilitate transitions between monomeric and dimeric forms, a binding−unbinding mechanism is hereby suggested: when JAM and the attachment proteins are mixed in solution, the trimer σ1 might occupy the interface of the first JAM when the receptor is in a monomeric form. This could be the most difficult step, and the proportion of a complex like this could be extremely small, considering the weaker interactions and faster dissociation of the σ1−1JAM complex compared to the homodimers. However, with the involvement of the second receptor protein, the total binding affinity is largely enhanced and the dissociation rate of the σ1−2JAM complex is lowered at the same time to a JAM−JAM interaction level. The number of such complexes might be increased more significantly than the number of

σ1−1JAM complexes. Finally, with the attachment of the last JAM molecule, the trimer protein is now caged by three receptors, and a tighter binding versus that of the homodimer is eventually presented. The whole process might be accomplished in a very short time, and the three steps possibly overlap with one another to generate the final σ1−JAM complex. The release of the trimer protein from the receptors is, hereby, assumed to be sequential as well. Compared to the rigid HB breaking behavior of the JAM−JAM complex, the flexible unbinding of the three groups of HBs in three consecutive steps could be presumed to be much slower. From a biological point of view, the tighter binding and slower dissociation rate of the σ1−JAM interactions might facilitate the stable adherence of the reovirus to the cell surface and help it to enter the cell as well. These investigations are expected to afford a basic model for studies of viral pathogenesis and provide a clue for manipulating reovirus tropism to enhance vector targeting research.

REFERENCES

1. Cavalli, A., Prota, A. E., Stehle, T., Dermody, T. S., Recanatini, M., Folkers, G., and Scapozza, L. (2004) A molecular dynamics study of reovirus attachment protein σ1 reveals conformational changes in σ1 structure. *Biophys. J. 86*, 3423–3431.
2. Tyler, K. L. (2001) Mammalian reoviruses. Fields Virology, 4th ed., pp 1729−1745, Lippincott Williams & Wilkins, Philadelphia.
3. Kobayashi, T., Antar, A. A. R., Boehme, K. W., Danthi, P., Eby, E. A., Guglielmi, K. M., Holm, G. H., Johnson, E. M., Maginnis, M. S., Naik, S., Skelton, W. B., Wetzed, J. D., Wilson, G. J., Chappell, J. D., and Dermody, T. S. (2007) A plasmid-based reverse genetics system for animal double-stranded RNA viruses. *Cell Host Microbe 1*, 147–157.
4. Duncan, R., Horne, D., Cashdollar, L. W., Joklik, W. K., and Lee, P. W. K. (1990) Identification of conserved domains in the cell attachment proteins of the three serotypes of reovirus. *Virology 174*, 399–409.
5. Nibert, M. L., Dermody, T. S., and Fields, B. N. (1986) Distinct pathways of viral spread in the host determined by reovirus S1 gene segment. *Science 233*, 770–774.
6. Bazzoni, G. (2003) The JAM family of junctional adhesion molecules. *Curr. Opin. Cell Biol. 15*, 525–530.
7. Furlong, D. B., Nibert, M. L., and Fields, B. N. (1988) σ1 protein of mammalian reoviruses extends from the surfaces of viral particles. *J. Virol. 62*, 246–256.
8. Fraser, R. D. B., Furlong, D. B., Trus, B. L., Nibert, M. L., Fields, B. N., and Steven, A. C. (1990) Molecular structure of the cell-attachment protein of reovirus: Correlation of computer-processed electron micrographs with sequence-based predictions. *J. Virol. 64*, 2990–3000.
9. Chappell, J. D., Prota, A. E., Dermody, T. S., and Stehle, T. (2002) Crystal structure of reovirus attachment protein σ1 reveals evolutionary relationship to adenovirus fiber. *EMBO J. 21*, 1–11.
10. Schelling, P., Guglielmi, K. M., Kirchner, E., Paetzold, B., Dermody, T. S., and Stehle, T. (2007) The reovirus σ1 aspartic acid sandwich: A trimerization motif poised for conformational change. *J. Biol. Chem. 282*, 11582–11589.
11. Kirchner, E., Guglielmi, K. M., Strauss, H. M., Dermody, T. S., and Stehle, T. (2008) Structure of reovirus σ1 in complex with its receptor junctional adhesion molecule-A. *PloS Pathog. 4*, e1000235.
12. Martìn-Padura, I., Lostaglio, S., Schneemann, M., Williams, L., Romano, M., Fruscella, P., Panzeri, C., Stoppacciaro, A., Ruco, L., Villa, A., Simmons, D., and Dejana, E. (1998) Junctional adhesion molecule, a novel member of the immunoglobulin superfamily that distributes at intercellular junctions and modulates monocyte transmigration. *J. Cell Biol. 142*, 117–127.
13. Barton, E. S., Connolly, J. L., Forrest, J. C., Chappell, J. D., and Dermody, T. S. (2001) Utilization of sialic acid as a coreceptor enhances reovirus attachment by multistep adhesion strengthening. *J. Biol. Chem. 276*, 2200–2211.
14. Barton, E. S., Forrest, J. C., Connolly, J. L., Chappell, J. D., Liu, Y., Schnell, F., Nusrat, A., Parkos, C. A., and Dermody, T. S. (2001) Junction adhesion molecule is a receptor for reovirus. *Cell 104*, 441–451.
15. Kostrewa, D., Brockhaus, M., D'Arcy, A., Dale, G. E., Nelboeck, P., Schmid, G., Mueller, F., Bazzoni, G., Dejana, E., Bartfai, T., Winkler, F. K., and Hennig, M. (2001) X-ray structure of junctional adhesion molecule: Structural basis for homophilic adhesion via a novel dimerization motif. *EMBO J. 20*, 4391–4398.
16. Prota, A. E., Campbell, J. A., Schelling, P., Forrest, J. C., Watson, M. J., Peters, T. R., Aurrand-Lions, M., Imhof, B. A., Dermody, T. S., and Stehle, T. (2003) Crystal structure of human junctional adhesion molecule 1: Implications for reovirus binding. *Proc. Natl. Acad. Sci. U.S.A. 100*, 5366–5371.
17. Cunningham, S. A., Arrate, M. P., Rodriguez, J. M., Bjercke, R. J., Vanderslice, P., Morris, A. P., and Brock, T. A. (2000) A novel protein with homology to the junctional adhesion molecule. Characterization of leukocyte interactions. *J. Biol. Chem. 275*, 34750–34756.
18. Sobocka, M. B., Sobocki, T., Banerjee, P., Weiss, C., Rushbrook, J. I., Norin, A. J., Hartwig, J., Salifu, M. O., Markell, M. S., Babinska, A., Ehrlich, Y. H., and Kornecki, E. (2000) Cloning of the human platelet F11 receptor: A cell adhesion molecule member of the immunoglobulin superfamily involved in platelet aggregation. *Blood 95*, 2600–2609.
19. Del Maschio, A., De Luigi, A., Martin-Padura, I., Brockhaus, M., Bartfai, T., Fruscella, P., Adorini, L., Martino, G., Furlan, R., De Simoni, M. G., and Dejana, E. (1999) Leukocyte recruitment in the cerebrospinal fluid of mice with experimental meningitis is inhibited by an antibody to junctional adhesional molecule (Jam). *J. Exp. Med. 190*, 1351–1356.
20. Springer, T. A. (1994) Traffic signals for lymphocyte recirculation and leukocyte emigration: The multistep paradigm. *Cell 76*, 301–314.
21. Bazzoni, G., Martinez-Estrada, O. M., Mueller, F., Nelboeck, P., Schmid, G., Bartfai, T., Dejana, E., and Brockhaus, M. (2000) Homophilic interaction of junctional adhesion molecule. *J. Biol. Chem. 275*, 30970–30976.
22. Woodfin, A., Reichel, C. A., Khandoga, A., Corada, M., Voisin, M. B., Scheiermann, C., Haskard, D. O., Dejana, E., Krombach, F., and Nourshargh, S. (2007) JAM-A mediates neutrophil transmigration in a stimulus-specific manner in vivo: Evidence for sequential roles for JAM-A and PECAM-1 in neutrophil transmigration. *Blood 110*, 1848–1856.
23. Naik, M. U., Naik, T. U., Suckow, A. T., Duncan, M. K., and Naik, U. P. (2008) Attenuation of Junctional Adhesion Molecule-A Is a Contributing Factor for Breast Cancer Cell Invasion. *Cancer Res. 68*, 2194–2203.
24. Guglielmi, K. M., Kirchner, E., Holm, G. H., Stehle, T., and Dermody, T. S. (2007) Reovirus binding determinants in junctional adhesion molecule-A. *J. Biol. Chem. 282*, 17930–17940.
25. Vedula, S. R., Lim, T. S., Kirchner, E., Guglielmi, K. M., Dermody, T. S., Stehle, T., Hunziker, W., and Lim, C. T. (2008) A comparative molecular force spectroscopy study of homophilic Jam-A interactions and Jam-A interactions with reovirus attachment protein σ1. *J. Mol. Recognit. 21*, 210–216.
26. Lim, T. S., Vedula, S. R. K., Hunziker, W., and Lim, C. T. (2008) Kinetics of Adhesion Mediated by Extracellular Loops of Claudin-2 as Revealed by Single Molecule Force Spectroscopy. *Mol. Biol. J. 381*, 681–691.
27. Lim, T. S., Vedula, S. R. K., Shi, H., Kausalya, P. J., Hunziker, W., and Lim, C. T. (2008) Dynamic response of Claudin-2 mediated adhesion to pH changes probed by single molecule force microscopy. *Exp. Cell Res. 314*, 2643–2651.
28. Vedula, S. R. K., Lim, T. S., Hunziker, W., and Lim, C. T. (2008) Mechanistic insights into physiological functions of cell adhesion proteins using single molecule force spectroscopy. *Mol. Cell. Biomech. 5*, 169–182.
29. Lim, T. S., Vedula, S. R. K., Kausalya, P. J., Hunziker, W., and Lim, C. T. (2008) Single molecular level study of claudin-1 mediated adhesion. *Langmuir 24*, 490–495.
30. Vedula, S. R. K., Lim, T. S., Shi, H., Kausalya, P. J., Lane, E. B., Rajagopal, G., Hunziker, W., and Lim, C. T. (2007) Molecular force spectroscopy of homophilic nectin-1 interactions. *Biochem. Biophys. Res. Commun. 362*, 886–892.
31. Zhang, B., Tan, V. B. C., Lim, K. M., and Tay, T. E. (2006) Molecular dynamics simulations on the inhibition of cyclin-dependent kinase 2 and 5 in the presence of activators. *J. Comput.-Aided Mol. Res. 20*, 395–404.
32. Zhang, B., Tan, V. B. C., Lim, K. M., and Tay, T. E. (2007) The activation and inhibition of cyclin-dependent kinase-5 by phosphorylation. *Biochemistry 46*, 10841–10851.
33. Zhang, B., Tan, V. B. C., Lim, K. M., Tay, T. E., and Zhuang, S. L. (2007) Study of the inhibition of cyclin-dependent kinases with roscovitine and indirubin-3′-oxime from molecular dynamics simulations. *J. Mol. Model. 13*, 79–89.

34. Zhang, B., Tan, V. B. C., Lim, K. M., and Tay, T. E. (2007) Significance of water molecules in the inhibition of cyclin-dependent kinase 2 and 5 complexes. *J. Chem. Inf. Model. 47*, 1877–1885.
35. Zhuang, S. L., Zou, J. W., Jiang, Y. J., Mao, X., Zhang, B., Liu, H. C., and Yu, Q. S. (2005) Some insights into the stereochemistry of inhibition of macrophage migration inhibitory factor with 2-fluoro-p-hydroxycinnamate and its analogues from molecular dynamics simulations. *J. Med. Chem. 48*, 7208–7214.
36. Orzechowski, M., and Cieplak, P. (2005) Application of steered molecular dynamics (SMD) to study DNA−drug complexes and probing helical propensity of amino acids. *J. Phys.: Condens. Matter 17*, S1627–S1640.
37. Sotomayor, M., and Schulten, K. (2007) Single-molecule experiments in vitro and in silico. *Science 316*, 1144–1148.
38. Hanasaki, I., Haga, T., and Kawano, S. (2008) The antigen-antibody unbinding process through steered molecular dynamics of a complex of an Fv frgagment and lysozyme. *J. Phys.: Condens. Matter 20*, 255238–255347.
39. Walton, E. B., Lee, S., and Van Vliet, K. J. (2008) Extending bell's model: How force transducer stiffness alters measured unbinding forces and kinetics of molecular complexes. *Biophys. J. 94*, 2621–2630.
40. Case, D. A., Pearlman, D. A., Caldwell, J. W., Cheatham, T. E., III, Wang, J., Ross, W. S., Simmerling, C. L., Darden, T. A., Merz, K. M., Stanton, R. V., Cheng, A. L., Vincent, J. J., Crowley, M., Tsui, V., Gohlke, H., Radme, R. J., Duan, Y., Pitera, J., Massova, I., Seibel, G. L., Singh, U. C., Weiner, P. K., and Kollman, P. A. (2007) AMBER 9, University of California, San Francisco.
41. Cornell, W. D., Cieplak, P., Bayly, C. I., Gould, I. R., Merz, K. M., Ferguson, D. M., Jr., Spellmeyer, D. C., Fox, T., Caldwell, J. W., and Kollman, P. A. (1995) A second generation force field for the simulation of proteins, nucleic acids and organic molecules. *J. Am. Chem. Soc. 117*, 5179–5197.
42. Jorgensen, W. L., Chandrasekhar, J., Madura, J. D., Impey, R. W., and Klein, M. L. (1983) Comparison of simple potential functions for simulating liquid water. *J. Chem. Phys. 79*, 926–935.
43. Darden, T., York, D., and Pedersen, L. (1993) An N.log(N) method for Ewald sums in large systems. *J. Chem. Phys. 98*, 10089–10092.
44. Ryckaert, J. P., Ciccotti, G., and Berendsen, H. J. C. (1997) Numerical integration of the Cartesian equations of motion of a system with constraints: Molecular dynamics of n-alkanes. *J. Comput. Phys. 23*, 327–341.
45. Massova, I., and Kollman, P. A. (2000) Combined molecular mechanical and continuum solvent approach (MM-PBSA/GBSA) to predict ligand binding. *Perspect. Drug Discovery Des. 18*, 113–135.
46. Heymann, B., and Grubmüller, H. (1999) AN02/DNP unbinding forces studied by molecular dynamics AFM simulations. *Chem. Phys. Lett. 303*, 1–9.
47. Heymann, B., and Grubmüller, H. (2001) Molecular dynamics force probe simulations of antibody/antigen unbinding: Entropic control and non-additivity of unbinding forces. *Biophys. J. 81*, 1295–1313.
48. Lu, H., and Schulten, K. (1999) Steered molecular dynamics simulation of conformational changes of immunoglobulin domain I27 interpret atomic force microscopy observations. *Chem. Phys. 247*, 141–153.
49. Jensen, M. Ø., Park, S., Tajkhorshid, E., and Schulten, K. (2002) Energetics of glycerol conduction through aquaglyceroporin GlpF. *Proc. Natl. Acad. Sci. U.S.A. 99*, 6731–6736.
50. Gohlke, H., Kiel, C., and Case, D. A. (2003) Insights into protein-protein binding by binding free energy calculation and free energy decomposition for the Ras-Raf and Ras-RalGDS complexes. *J. Mol. Biol. 330*, 891–913.
51. Sanner, M. F., Olson, A. J., and Spehner, J. C. (1996) Reduced surface: An efficient way to compute molecular surfaces. *Biopolymers 38*, 305–320.
52. Sitkoff, D., Sharp, K. A., and Honig, B. (1994) Accurate calculation of hydration free energies using macroscopic solvent models. *J. Phys. Chem. 98*, 1978–1988.
53. Bell, G. I. (1978) Models for the specific adhesion of cells to cells. *Science 200*, 618–627.
54. Merkel, R., Nassoy, P., Leung, A., Ritchie, K., and Evans, E. (1999) Energy Landscapes of Receptor-Ligand Bonds Explored with Dynamic Force Spectroscopy. *Nature 397*, 50–53.
55. Sulchek, T. A., Friddle, R. W., Langry, K., Lau, E. Y., Albrecht, H., Ratto, T. V., DeNardo, S. J., Colvin, M. E., and Noy, A. (2005) Dynamic force spectroscopy of parallel individual Mucin1-antibody bonds. *Proc. Natl. Acad. Sci. U.S.A. 102*, 16638–16643.
56. Evans, E. A., and Calderwood, D. A. (2007) Forces and Bond Dynamics in Cell Adhesion. *Science 316*, 1148–1153.
57. Evans, E. A., and Ritchie, K. (1997) Dynamic strength of molecular adhesion bonds. *Biophys. J. 72*, 1541–1555.
58. Izrailev, S., Stepaniants, S., Balsera, M., Oono, Y., and Schulten, K. (1997) Molecular dynamics study of unbinding of the avidin-biotin complex. *Biophys. J. 72*, 1568–1581.